Recent Enhancements and Studies of Isogeometric Shells in LS-DYNA

Lukas Leidinger[1], Stefan Hartmann[1], Qining Tang[1], Philipp Bähr[2], Silke Sommer[2], Christian Ilg[1], Werner Feix[1], Filipe Andrade[1]

[1]DYNAmore GmbH, an ANSYS Company
Industriestr. 2, 70565 Stuttgart, Germany

[2]Fraunhofer - Institut für Werkstoffmechanik IWM
Wöhlerstr. 11, 79108 Freiburg, Germany

1 Introduction

Isogeometric Analysis (IGA) [1] is a Finite Element Analysis (FEA) technology that uses spline basis functions known from Computer Aided Design (CAD) to describe the geometry and the solution field. Employing such spline basis functions with higher order and higher continuity may yield several advantages such as an easier transition from CAD to analysis, a more accurate geometry description, smooth solution fields or a larger time step in explicit analysis. In fact, only the higher-continuity property of splines enables the concept of trimming (ubiquitous in CAD) to be used in explicit analysis with a feasible time step size [2].
Over the last years, the trimmed IGA shell capabilities in ANSYS LS-DYNA® were consistently enhanced and reached a high level of maturity [3,4] as demonstrated in a recent study by Bauer et al. [5]. In that study, a Body in White (BIW) was modeled with hundreds of trimmed IGA shell components (using ANSA [6]) and successfully implemented in hybrid IGA/FEA full vehicle crash simulations. Comparisons and conclusions were made on a global vehicle level.
In the present contribution, we aim at more detailed studies on a smaller coupon level. In Section 2, we use KS2 and lap shear specimens to study the behavior of ***CONSTRAINED_INTERPOLATION_SPOTWELD (*CIS)** joints between IGA shell models. We take a ***CIS** model originally calibrated for FEA shells, apply it to IGA shell models and compare the results with experiments and pure FEA simulations. In Section 3, we study the elasto-plastic, damage and failure behavior of IGA shells on a set of representative test specimens. We take a ***MAT_024** material with GISSMO originally created for FEA shells, apply it directly to IGA shell models and compare the IGA results with pure FEA simulations. Referring back to full vehicle crash simulations, it is state of the art to consider the material history, e.g. from sheet metal forming processes, in such crash models. In Section 4, we therefore introduce ***INCLUDE_STAMPED_PART** as a convenient tool to map material history data onto IGA shell models directly within LS-DYNA. We close this paper with a short conclusion and an outlook to future work.

2 Joint Modeling with *CONSTRAINED_INTERPOLATION_SPOTWELD (SPR3)

Joining technologies like spotwelds and self-piercing rivets play an essential role in automotive, aerospace and railroad products. One way to model such point-based joints in LS-DYNA is the use of ***CONSTRAINED_INTERPOLATION_SPOTWELD** (***CIS**, prior notation ***CONSTRAINED_SPR3** still works). With this keyword, FE nodes of the involved sheets are collected within a predefined radius and constrained through a substitute SPR3 model to represent the joint. In LS-DYNA, ***CIS** can also be applied to IGA shells via an interpolation mesh [7]. Detailed information about ***CIS**, the attractive benefits, the keyword usage and the functionality with IGA shells were already provided in previous LS-DYNA conference publications [4,8,9] and the LS-DYNA manual [10] and shall not be repeated here for brevity.
In the hybrid IGA/FEA BIW model [5] mentioned above, hundreds of spotwelds between IGA shells were modeled with ***CIS**. These ***CIS** definitions and the corresponding material parameters were directly taken from the pure FEA model without further adjustments. The question we want to answer here is whether the ***CIS** definitions originally created for FEA shell models also provide accurate results when used on IGA shell models with higher order, higher continuity and different interpolation mesh size. We therefore performed detailed KS2 and lap shear test simulations with IGA shells and compared them to results from both FEA shell simulations and experiments.

Figure 1 shows the test configurations with KS2 specimens loaded under different angles and the corresponding force-displacement curves from the experiments. The experimental data represents a self-piercing riveting (SPR) joint between two 1.5mm thick HCT780X and HC340LA sheets from the AiF/FOSTA research project IGF-No. 20116 N / P 1262 [12]. The FEA and the IGA shell models of the KS2 specimens are depicted in Fig. 2. The FEA models use fully-integrated shell elements (ELFORM=16) with a mesh size of 2.5mm. The IGA models use quadratic Reissner-Mindlin shell elements (ELFORM=3) with reduced Gauss integration (IRL=0) and also 2.5mm element size. They are modeled through multiple untrimmed patches with matching discretization, coupled in a strong sense. In this AiF/FOSTA research project, a **`*CIS`** definition including material parameters was calibrated for FEA shell elements. We use this **`*CIS`** definition without modifications directly for our IGA shell models. It should be noted that a search radius of 6.0mm, which corresponds to approximately twice the rivet diameter, was used in the **`*CIS`** definition for both the IGA and FEA model. This is necessary to reproduce the load-bearing behavior of the KS2-0° specimen in the FEA model. More information about the specific **`*CIS`** model (model 2 [10]), the simulation setup and the experimental database can be found in the original publication by Bähr et al. [11].

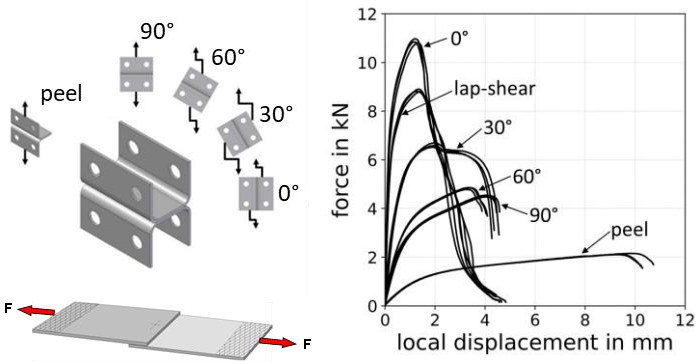

Fig.1: KS2 and lap shear test setup [12] (left) and experimental force-displacement results [12] (right).

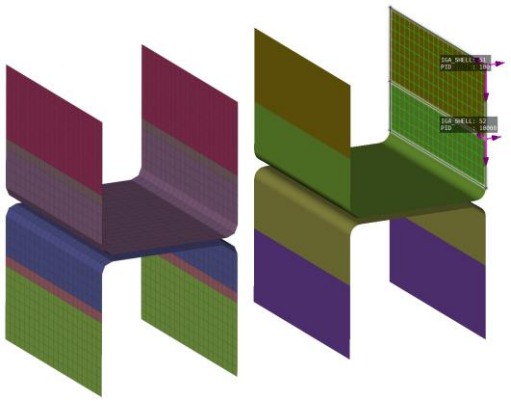

Fig.2: KS2 specimen: FEA shell model (left) and IGA shell model (right) with same element size [11].

Figure 3 compares the results of the IGA shell model with the results of the FEA shell model and the experimental tests. For most test cases, we observe excellent agreement between IGA, FEA and experimental results. Maximum forces and energy absorption are well captured by the simulations. For the KS2-60°, -90° and peel specimens, the fracture displacement of the IGA models is slightly higher compared to the FEA model. For the KS2-30° specimen, deviations in the plastic behavior of the IGA model are observed with a lower maximum force and larger fracture displacement. For the lap shear test, the FEA and the IGA model show similar results with a higher maximum load-bearing capacity compared to the experimental result. This is because the **`*CIS`** model was calibrated with respect to the KS2-0° results, see [11] for more details. Fig. 4 shows the deformed FEA and IGA models of a KS2-0° specimen with a reduced **`*CIS`** radius of 3.0mm which is closer to the real size of a rivet or spotweld. These results indicate that the IGA model is able to capture the local deformation and the local strains more accurately than the FEA model for the same element size (2.5mm for FEA and IGA). Please note that the IGA model in Fig. 4 is visualized by an interpolation mesh with 2x2 linear elements per IGA element.

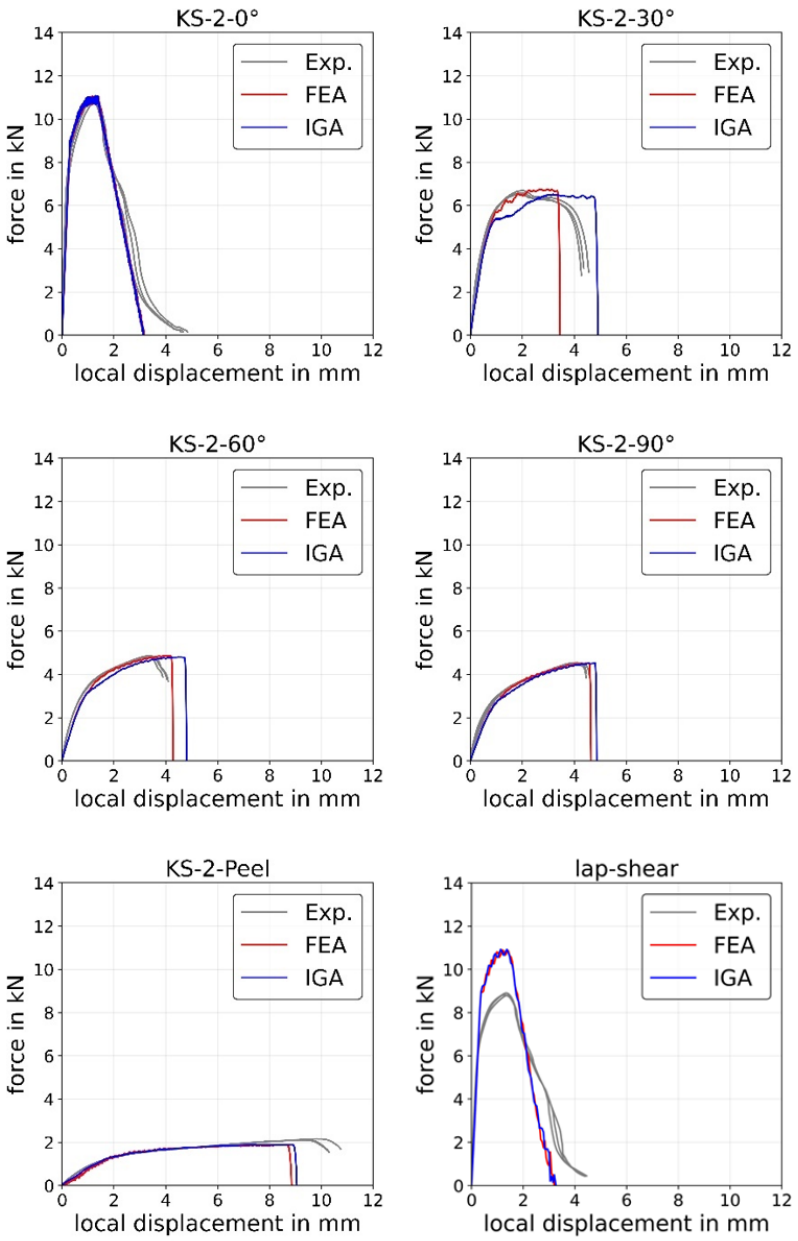

Fig.3: Force-displacement results for KS2 and lap shear tests: Experiment vs. FEA vs. IGA [11].

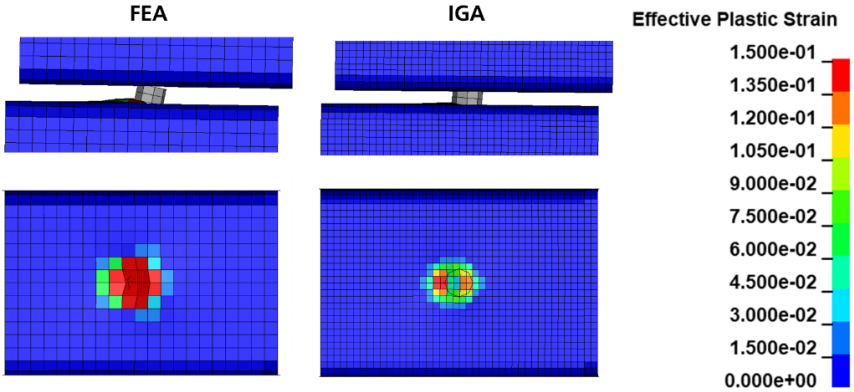

Fig.4: Deformation and effective plastic strain of KS2 0° models for FEA and IGA [11]. The same element size of 2.5mm is used for the FEA and the IGA model. IGA results are visualized on an interpolation mesh with 2x2 linear elements per IGA element.

Here, only a part of the results of the conducted study is shown. Complete results, further component test cases, and more detailed discussions can be found in the original publication [11].
Finally, we would like to highlight that we performed the same KS2 and lap shear tests with the *CIS definition (model 1 [10]) of the previously mentioned IGA/FEA hybrid BIW model [5] and obtained similar agreement between IGA and FEA models.

3 Damage and Failure Modeling with *MAT_024 and GISSMO

Similar to the connections in the previous section, we here aim to understand whether material and damage-failure cards calibrated for FEA shells can also provide accurate results when used with IGA shell models. In Leidinger et al. [9], we already compared FEA and IGA shell models of a standard tensile test ran with ***MAT_024** and DIEM (Damage Initiation and Evolution Model) [10,13] and reported very good agreement. We also discussed the required element erosion scheme and the importance of an appropriate characteristic element length for IGA with a higher-order and higher-continuity basis. In the present study, we extend our tests to a wider range of specimens and focus on ***MAT_024** with GISSMO (Generalized Incremental Stress-State dependent damage Model) [10,13].
At the DYNAmore Material Competence Center (MCC), material cards for ***MAT_024** and ***MAT_ADD_DAMAGE_GISSMO** are determined and calibrated with the set of test specimens shown in Fig. 5 (left). These specimens are well-selected to capture a wide range of stress triaxialities and discretized with a relatively fine mesh size of 0.5mm. To finally regularize the material card and thus the FEA model response across different mesh sizes, the large tensile specimen shown in Fig. 5 (right) is simulated with mesh sizes of 0.5, 1.0, 2.5, 5.0 and 10mm.

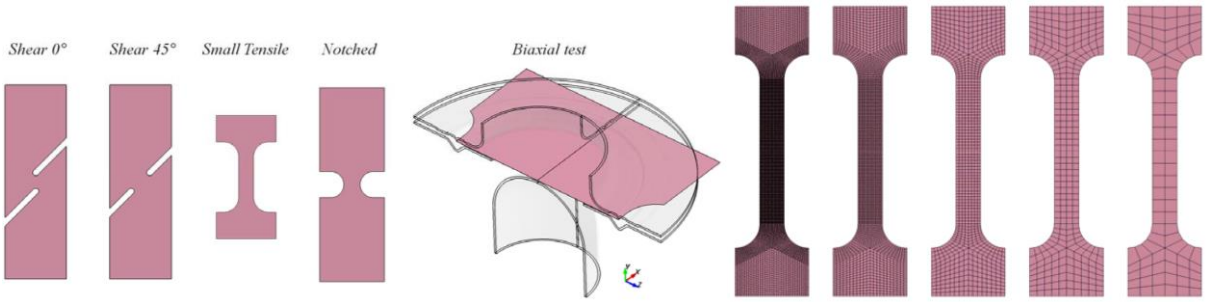

*Fig.5: Set of test specimens used for material calibration (left) and large tensile test with different mesh sizes used for regularization (right) of **MAT_024 and GISSMO cards [13].*

To assess the behavior of IGA shells, we take a ***MAT_024** and GISSMO card of a DP800 steel originally created for FEA shell models and rerun the set of test specimens with trimmed NURBS-based IGA shell models. The utilized ***MAT_024** material card does not consider strain rate-dependency. The ***MAT_ADD_DAMAGE_GISSMO** card contains a failure strain curve, a material instability curve, a damage-related stress fadeout curve, and a regularization curve.
The FEA models use linear fully-integrated shell elements (ELFORM=16). The IGA models use quadratic Reissner-Mindlin shell elements (ELFORM=3) with reduced Gauss integration (IRL=0). Thus, the FEA and the IGA shell elements both have 2x2 in-plane integration points and both use NIP=5 out-of-plane integration points. An element erosion criterion for IGA shells can be defined via the parameter NIPF in ***DEFINE_ELEMENT_EROSION_IGA**. As in Leidinger et al. [9], the default NIPF=1 is used, indicating that a layer is considered as failed as soon as one integration point of the layer is failed. The parameter NUMFIP in ***MAT_ADD_DAMAGE_GISSMO** is not altered for IGA.
For comparisons, we use the same element size for the IGA and the FEA shell models. Figure 6 exemplarily depicts the FEA and IGA shear 0° models with 0.5mm element size. With this level of mesh fineness, spurious cross-talk effects across the trimming features of IGA shell models are small, if not negligible, see [14] for more information. Furthermore, the IGA models are defined such that the patch boundaries conform with the convex hull of the specimen. This allows applying ***BOUNDARY_SPC** and ***BOUNDARY_PRESCRIBED_MOTION** directly to the control points located at the top and bottom edges, in a strong sense as also done for the FEA models. For the evaluation, engineering stresses are computed from cross-section forces measured at significant locations and engineering strains from the displacements of two significant points on the specimens.

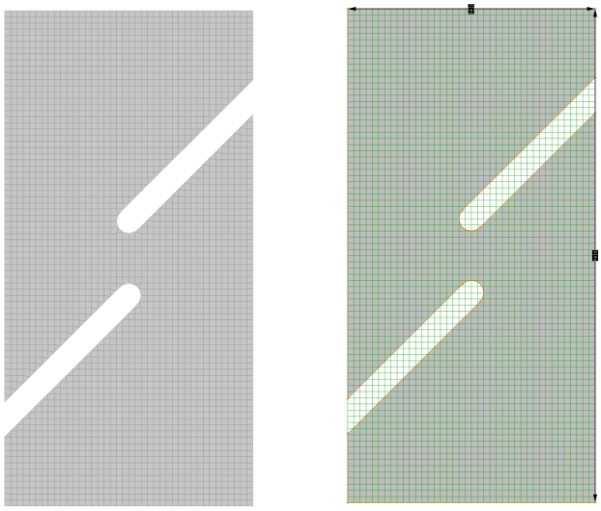

Fig.6: Shear 0° specimen with 0.5mm element size: FEA shell model (left) and trimmed IGA shell model (right).

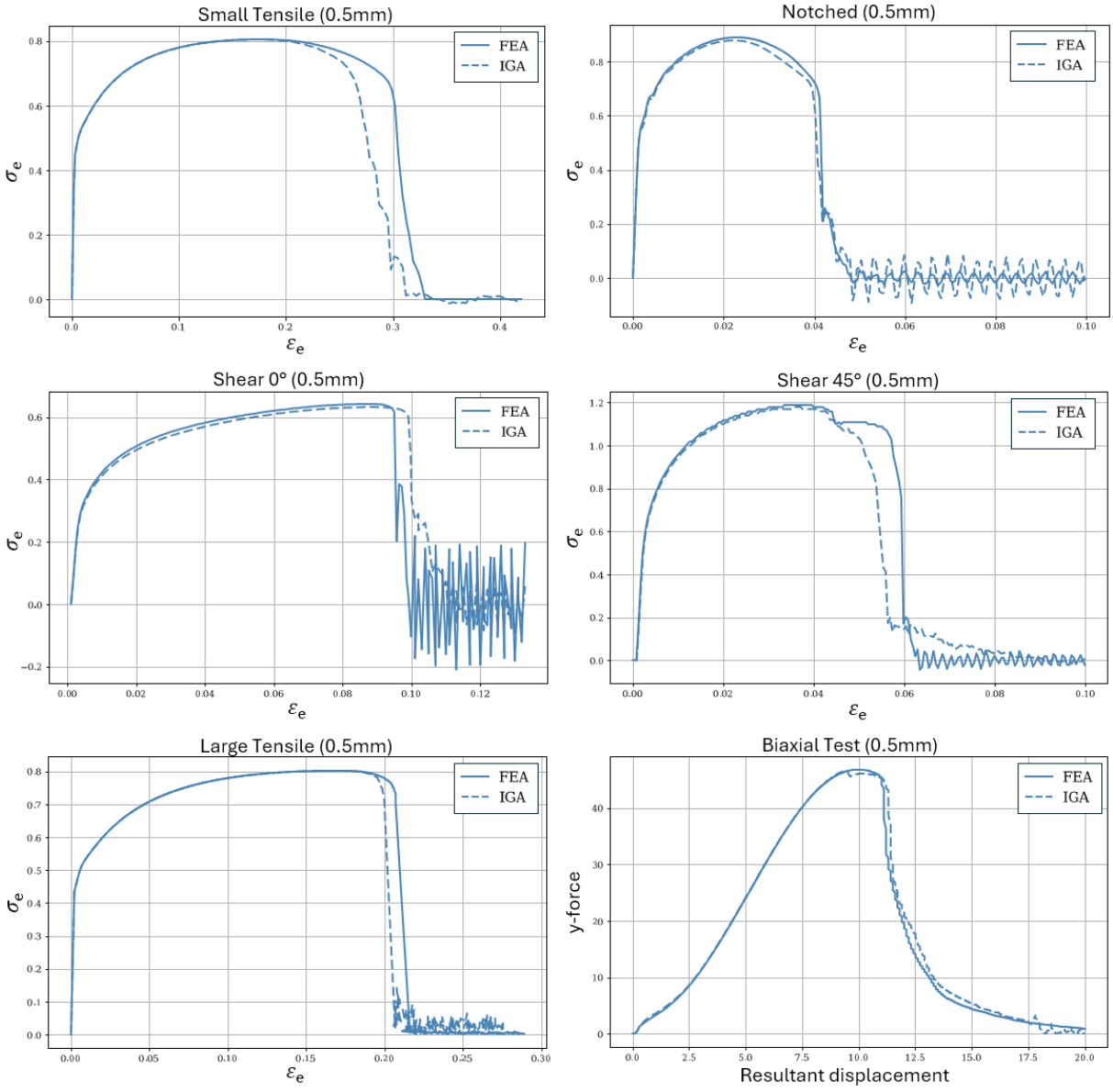

Fig.7: Comparison of FEA and IGA results for the 0.5mm test specimens.

Stress-strain or force-displacement curves of all FEA and IGA specimens with 0.5mm element size are compared in Figure 7. As can be seen, good overall agreement is obtained between FEA and IGA, especially in the elasto-plastic domain until the point of maximum stress and force. After damage initiation, the IGA models tend to damage and fail (slightly) earlier, except for the shear 0° specimen. Figures 8 and 9 show the deformed geometries with the corresponding effective plastic strains immediately before the first element failure and after complete rupture, respectively. Overall, the plastic strain and failure patterns agree well between FEA and IGA. The slightly higher strains and the more pronounced localization in the IGA models in Fig. 8, confirm the softer behavior after the maximum stress and force observed in Fig. 7.

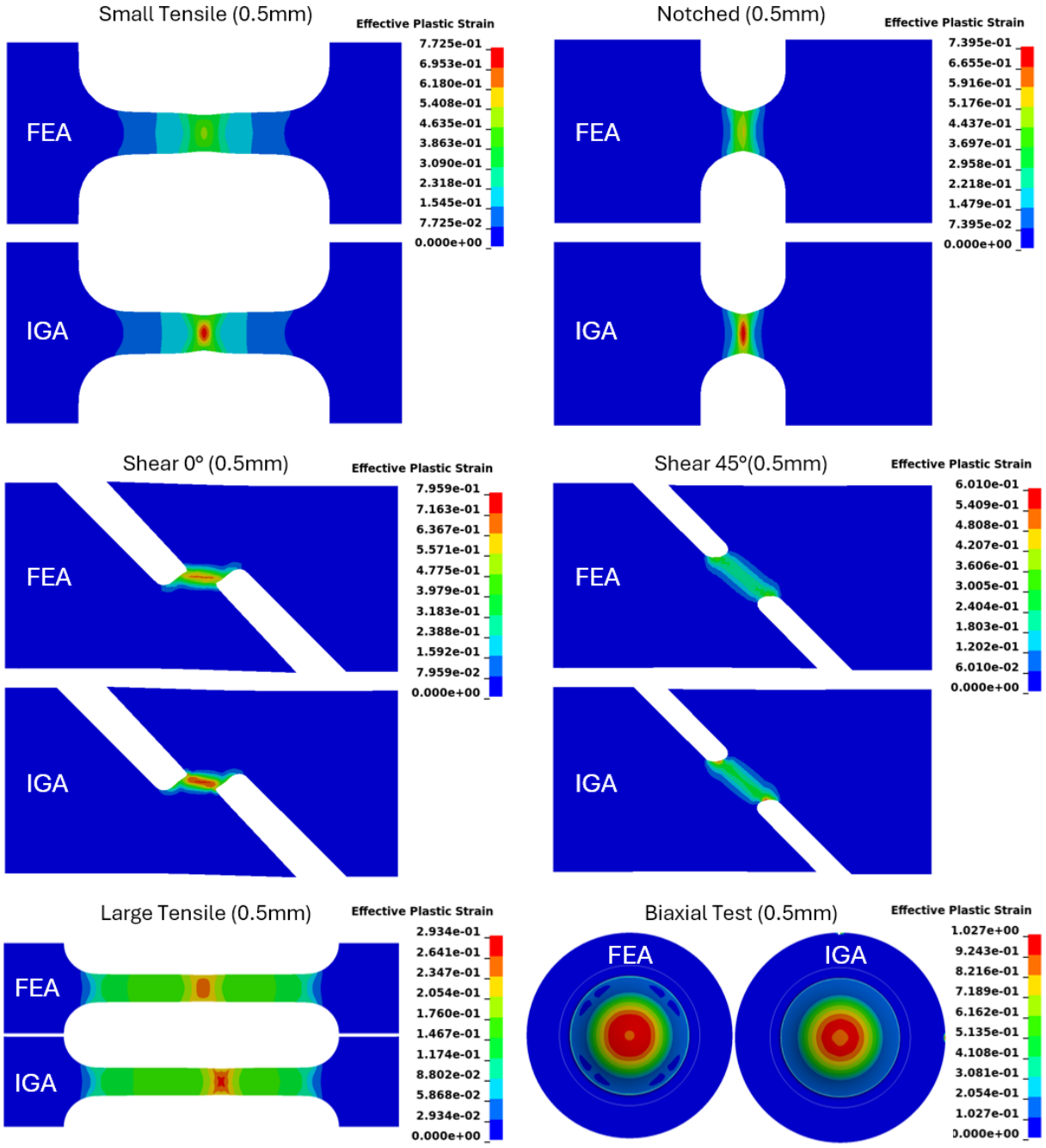

Fig.8: Comparison of deformed FEA and IGA models slightly before first element failure.

This behavior indicates that the IGA models capture localization more accurately. To confirm this, we simulate the large tensile specimen with varying element size and a GISSMO card without the regularization curve and without the element size-dependent stress fadeout curve. That is, no element size-dependency is considered in this GISSMO card. The comparison of FEA and IGA results is

depicted in Fig. 10 (left), clearly showing softer behavior with finer mesh sizes after the point of maximum stress. This means that IGA allows a larger element size for the same results, or in other words, gives better results for the same element size. This seemingly better behavior could be considered in a material calibration and regularization specifically for IGA shell elements. For completeness, the results with the original GISSMO card including regularization are shown in Fig. 10 (right), clearly showing that regularization is also effective for the IGA models.

In conclusion, this study demonstrates that an existing material card **`*MAT_024`** with GISSMO originally created for FEA shells can also provide good results for IGA shell models. However, because IGA shows a more pronounced localization and a slightly softer response in the damage evolution phase, material cards specifically generated for IGA may provide even better accuracy. Users are advised to take this decision based on their own tests and for their specific materials.

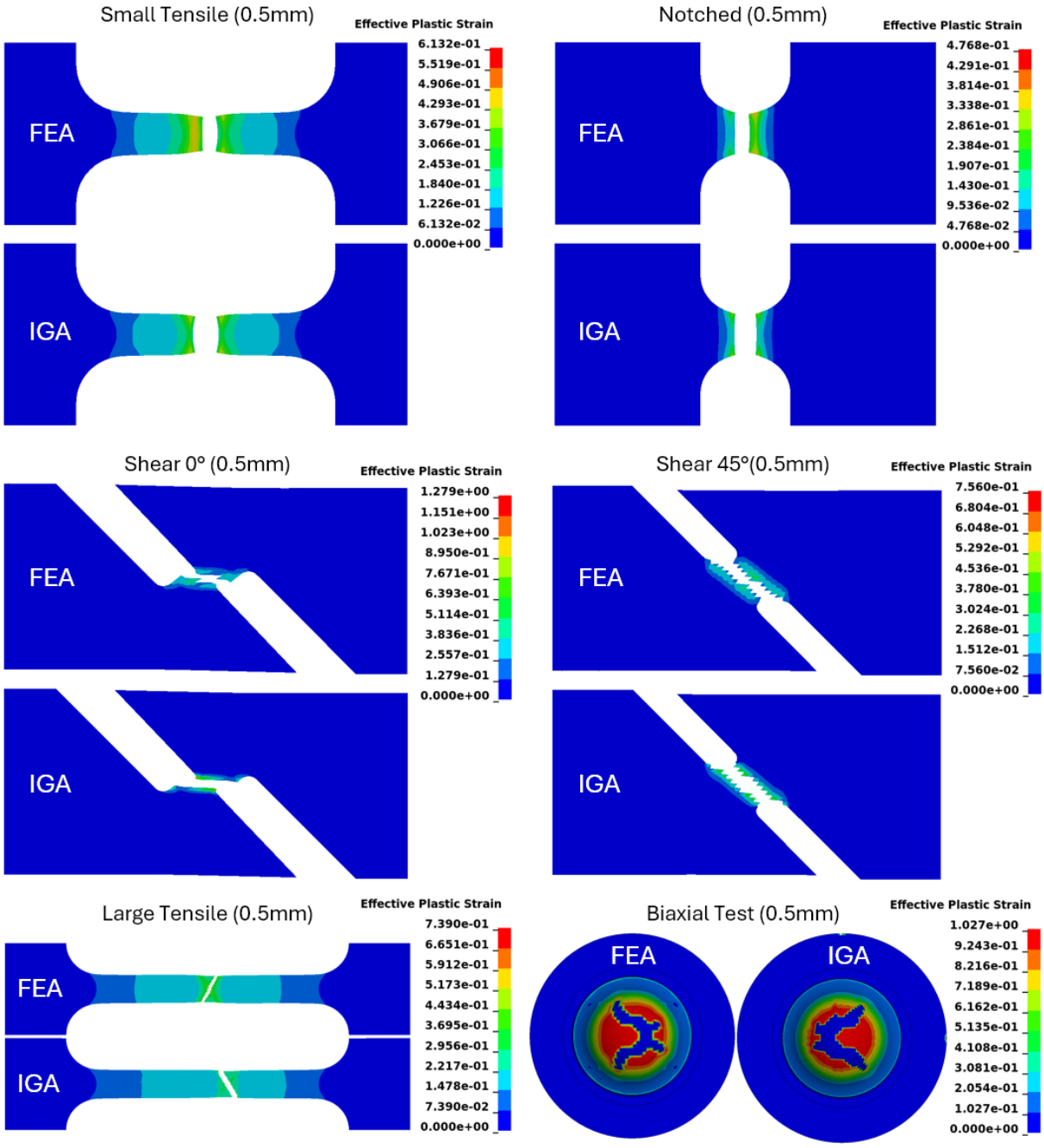

Fig.9: Comparison of deformed FEA and IGA models after complete rupture.

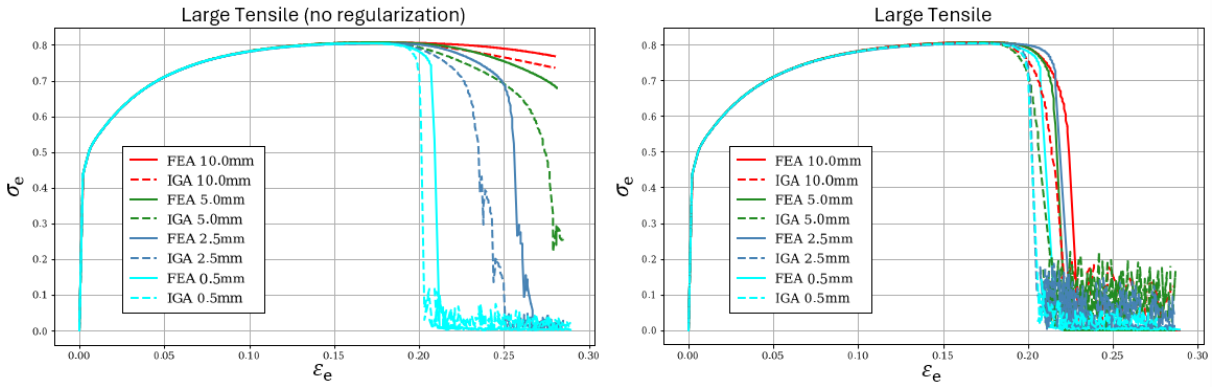

Fig.10: Large tensile specimen: Comparison of FEA and IGA results for different element sizes without (left) and with regularization in GISSMO (right).

4 Mapping of Material History Data with *INCLUDE_STAMPED_PART

A new and very convenient possibility to map material history data onto IGA shell models shall be briefly introduced here. Instead of using external tools to map data from a source mesh (e.g. forming simulation) to a target mesh (e.g. crash simulation), this mapping can be done internally in LS-DYNA through the keyword ***INCLUDE_STAMPED**. Starting from LS-DYNA R15, ***INCLUDE_STAMPED** with the option **_PART** can also be used to map data from an FEA part to an IGA part as shown in Fig. 11. This keyword takes the source mesh (here S-Rail_FEA_forming.dynain) as an input and refers to the PID of the IGA source part (here PID=3 in S-Rail_IGA_PID3.key). In this example, the **_MATRIX** option is used, which allows defining the transformation matrix between the source and the target. Since the source and the target part are already aligned here, the transformation matrix (R11-R33) is the identity matrix and the translational distance (XP, YP, ZP) is zero.
Figure 12 shows the results of an FEA forming simulation (source) and the corresponding data mapped with ***INCLUDE_STAMPED_PART** onto an IGA crash component (target). It should be noted that ***INCLUDE_STAMPED_PART** for IGA is currently limited to FEA source meshes but can be extended to IGA source meshes upon request.

```
*INCLUDE
S-Rail_IGA_PID3.key
*INCLUDE_STAMPED_PART_MATRIX
$  FILENAME                                                                  |
S-Rail_FEA_forming.dynain
$       PID|     THICK|     PSTRN|    STRAIN|    STRESS|    INCOUT|                RMAX|
         3          0          0          0          0          0                  0.
$       R11|       R12|       R13|        XP|    TENSOR|    THKSCL|
         1          0          0          0          0
$       R21|       R22|       R23|        YP|
         0          1          0          0
$       R31|       R32|       R33|        ZP|
         0          0          1          0
$                        PERCELE|                        ISRCOUT|
                              0.                               1
```

*Fig.11: Using the ***INCLUDE_STAMPED_PART** keyword to map data onto an IGA shell part.*

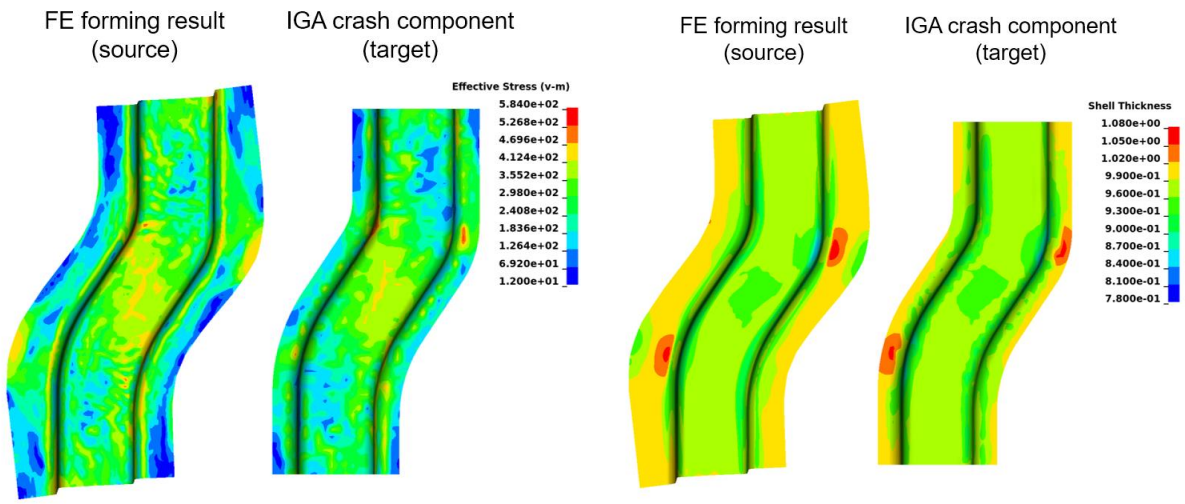

Fig.12: Mapping of effective stress and shell thickness from an FEA forming simulation (source, fine mesh) to an IGA crash component (target, coarser mesh).

5 Conclusion and Outlook

Motivated by recent investigations of hybrid IGA/FEA crash models on a global vehicle level [5], the aim of this paper was to perform more detailed studies of IGA shells on a coupon level. We particularly addressed the question whether joint definitions (***CONSTRAINED_INTERPOLATION_SPOTWELD**) and material cards (***MAT_024** with GISSMO) originally calibrated for FEA shell models can provide accurate results when directly applied to IGA shell models. For this purpose, we performed (i) KS2 and lap shear tests for IGA shell models connected through ***CIS** and (ii) coupon tests with ***MAT_024** and GISSMO cards on a well-selected set of specimens covering a wide range of stress triaxialities, both until failure.

In both studies we observed good overall agreement between the IGA and the FEA shell models, but also the tendency that IGA models capture local effects more accurately, partially leading to slightly softer responses for the same element size. Thus, even better accuracy may be achieved when calibrating ***CIS** and material cards specifically for IGA shells. As a next step, we plan to perform such calibrations for IGA shell models, rerun the presented test cases and assess the accuracy improvements. Nevertheless, the presented studies indicate that applying existing ***CIS** and material cards to IGA shells is still a good starting point.

In the future, similar studies shall be performed for other joining technologies, different material and damage cards, and for (trimmed) IGA solids, see the contribution by Hartmann et al. [15]. We also encourage users to perform similar studies and to share their experiences.

In this paper, we also briefly introduced the new possibility of mapping material history data onto IGA shells directly in LS-DYNA using ***INCLUDE_STAMPED_PART**. This new capability makes the mapping process for IGA shells much simpler and more convenient. Upon request, the current functionality can be extended in the future.

6 Acknowledgement

Part of the work presented in this paper was developed within the project “DigiTain – Digitalization for Sustainability”. The project “DigiTain” is funded by the European Union and the German Federal Ministry for Economy and Climate Protection within the framework of the economic stimulus package no. 35c in module b under grant #19S22006c on the basis of a decision by the German Bundestag.

7 Literature

[1] Hughes, T.J.R., Cottrell, J.A., Bazilevs, Y.: “Isogeometric Analysis: CAD, finite elements, NURBS, exact geometry, and mesh refinement”, Computer Methods in Applied Mechanics and Engineering, Vol. 194, 2005, 4135-4195.

[2] Leidinger, L., “Explicit Isogeometric B-Rep Analysis for Nonlinear Dynamic Crash Simulations”, PhD Thesis, Technical University of Munich, Germany, 2020.

[3] Hartmann, S., Leidinger, L.F., Benson, D., Li, L., Nagy, A., Pigazzini, M.: “Enabling the Analysis of Topologically Connected Multi-Patch Trimmed NURBS Shells in LS-DYNA”, 12th European LS-DYNA Conference 2019, Koblenz, Germany.
[4] Leidinger, L., Hartmann, S., Benson, D., Nagy, A., Rorris, L., Chalkidis, I., Bauer, F.: “Hybrid IGA/FEA Vehicle Crash Simulations with Trimmed NURBS-based Shells in LS-DYNA”, 13th European LS-DYNA Conference 2021, Ulm, Germany.
[5] Bauer, F., Yugeng, T., Leidinger, L., Hartmann, S.: “Experience with Crash Simulations using an IGA Body in White”, 14th European LS-DYNA Conference 2023, Baden-Baden, Germany.
[6] Rorris, L., Chalkidis, I.: “Latest ANSA developments for IGA modeling”, 14th European LS-DYNA Conference 2023, Baden-Baden, Germany.
[7] Hartmann, S., Benson, D., Lorenz, D.: “About Isogeometric Analysis and the new NURBS-based Finite Elements in LS-DYNA”, 8th European LS-DYNA Conference 2011, Strasbourg, France.
[8] Hartmann, S., Leidinger, L., Benson, D., Nagy, A., Pigazzini, M., Li, L., Nguyen, L.: “Isogeometric Analysis in LS-DYNA R13 – key steps towards industrial applications”, 13th European LS-DYNA Conference 2021, Ulm, Germany.
[9] Leidinger, L., Hartmann, S., Bauer, F., Benson, D., Nagy, A., Li, L., Pigazzini, M., Nguyen, L.: "Enabling Productive Use of Isogeometric Shells in LS-DYNA", 14th European LS-DYNA Conference 2023, Baden-Baden, Germany.
[10] ANSYS: LS-DYNA Keyword User’s Manual R15.0: Volume I (2024), https://lsdyna.ansys.com/manuals/
[11] Bähr, P., Leidinger, L., Sommer, S., Hartmann, S.: “Validation of the *CONSTRAINED_SPR3 joint formulation for isogeometric shell models”, Stuttgart Conference on Automotive Production 2024, Stuttgart, Germany.
[12] Rochel, P., Sommer, S., Olfert, V., Meschut, G.: “Impact of production-related tolerances of the failure and deformation behavior of mechanical joints under crash loading”, Final report IGF-No. 20116 N, in Forschung für die Praxis P 1262. Düsseldorf: Forschungsvereinigung Stahlanwendung e. V., 2021.
[13] Andrade, F., Feucht, M., Haufe, A.: “On the Prediction of Material Failure in LS-DYNA: A Comparison Between GISSMO and DIEM”, 13th International LS-DYNA Users Conference, Detroit, 2014.
[14] Lian, Z., Leidinger, L., Hartmann, S., Bauer, F., Wüchner, R.: “Towards the Solution of Cross-Talk in Explicit Isogeometric B-Rep Analysis”, 14th European LS-DYNA Conference 2023, Baden-Baden, Germany.
[15] Hartmann, S., Leidinger, L., Bauer, F., Benson, D., Li, L., Nagy, A., Nguyen, L., Pigazzini, M.: “Updates on trimmed IGA B-Spline Solids”, 2024 International LS-DYNA Conference 2024, Metro Detroit, Michigan, USA.